

Origin of rebounds with a restitution coefficient larger than unity in nanocluster collisions

Hiroto Kuninaka^{1,*} and Hisao Hayakawa²

¹*Faculty of Education, Mie University, Tsu city, Mie, Japan, 514-8507*

²*Yukawa Institute for Theoretical Physics, Kyoto University, Sakyo-ku, Kyoto, Japan, 606-8502*

(Dated: February 21, 2022)

We numerically investigate the mechanism of super rebounds for head-on collisions between nanoclusters in which the restitution coefficient is larger than unity. It is confirmed that the temperature and the entropy of the nanoclusters decrease after the super rebounds by our molecular dynamics simulations. It is also found that the initial metastable structure plays a key role for the emergence of the super rebounds.

PACS numbers: 82.60.Qr, 45.50.-j, 45.70.-n, 83.10.Rs

I. INTRODUCTION

Nanoclusters are technologically important for the construction of nanodevices. Because the size of nanoclusters is mesoscopic, thermodynamic properties of such materials are still not well understood[1], though the methods to make nanoclusters such as adiabatic expansion through a nozzle and a laser ablation technique are well established.[2]

Dynamics of nanoclusters are extensively investigated from both scientific and technological interest. There are many numerical studies on cluster-cluster and cluster-surface collisions based on the molecular dynamics simulation. [3–18] We observe variety of rebound processes for such systems caused by the competition between the attractive interaction and the repulsive interaction of two colliding bodies. Binary collisions of identical clusters cause coalescence, scattering, and fragmentation depending on the cluster size and the impact energy. [11, 12] On the other hand, cluster-surface collisions induce soft landing, embedding, and fragmentation.[7, 15, 16] The attractive interaction plays crucially important roles in collisions of nanoclusters, so that the modeling of the cohesive collisions in various scale are actively discussed in these days.[19–21] .

However, the attractive interaction can be reduced by some combinations of the two interacting objects and the relative configuration of colliding molecules.[22] Awasthi *et al.* introduced a modified Lennard-Jones model to simulate the rebound process of a Bi cluster onto a SiO₂ surface[10], in which they introduced a cohesive parameter to reduce the attractive interaction between different atoms on the surface. There exists a corresponding experiment on the rebound process of Bi nanoclusters on a Si surface with the aid of a V-shaped template etched on a silicon wafer.[3] This suggests that the modified Lennard-Jones clusters can approximately describe collisions of real clusters. Similarly, recent papers have

reported that surface-passivated Si nanoclusters exhibit elastic rebounds on Si surface due to the reduction of the attractive interaction between the surfaces.[8, 23, 24] In particular, Saitoh *et al.* confirmed that the behavior in collisions of modified Lennard-Jones clusters is similar to that of H-passivated Si clusters from their simulation.[24] These results also support that the modified Lennard-Jones model can be regarded as a simplified model of nanoclusters.

In general, thermal fluctuation also plays an important role for small systems such as nanoclusters. Indeed, the present authors carried out the molecular dynamics simulation of colliding thermally activated modified Lennard-Jones clusters to investigate the impact phenomena and found the existence of the “super-rebound” in which the restitution coefficient is larger than unity.[6] Recently, it has been reported that such a rebound can be observed in a molecular dynamics simulation of a collision of Cu nanoparticles on a rigid wall.[5] In addition, another research group has reported that large recovery strain after loading (called super-elasticity) can be found in a small system.[25] Although there is a possibility that such an anomalous mechanical property of small systems is also concerned with the emergence of “super rebounds”, the underlying mechanism for the “super rebounds” is still unclear.

In macroscopic systems, the restitution coefficient larger than unity can be observed in oblique collisions between a hard sphere and a soft elastic plate [26, 27], which differs from the super rebound. Indeed, the restitution coefficient can easily become larger than unity if the rebound direction is changed in oblique collisions. As another example, a recent study reported that the large-scale magnetized plasmoids can gain the increased kinetic energy after collision in the heliosphere.[28] On the contrary, in microscopic systems such as nanoclusters, the true “super rebounds” can be observed in normal collisions, which implies that a part of thermal energy is converted to macroscopic degrees of freedom. This may imply a possibility to make a nanoscale object which extracts work from its internal energy. Although the averaged behavior of the restitution coefficient against the

*E-mail: kuninaka@edu.mie-u.ac.jp

relative impact speed can be approximately understood by the macroscopic theory of cohesive collisions,[6, 19] the mechanism of curious energy transfer against intuition of the thermodynamics is important to both fundamental physics and energy technology.

The aim of this paper is to study the mechanism of the super rebounds from the viewpoint of the energy transfer between the microscopic and the macroscopic degrees of freedom. For this purpose, we investigate the characteristics of thermodynamic functions such as temperature and entropy in the super rebounds based on the molecular dynamics simulation. In addition, we also investigate the change in structures of the colliding nanoclusters characterizing super rebounds by the introduction of Steinhardt's order parameter[29] and some related geometrical order parameters.

The organization of this paper is as follows. In the next section, we introduce our nanocluster model. In Sec. III we show the results of our molecular dynamics simulations. In Sec. IV we discuss the reason why super rebounds can be observed in our simulation. Section V is devoted to the summary of this work. In Appendices A and B, we explain the method of calculating entropy in our simulation and how to calculate Steinhardt's order parameters, respectively.

II. MODEL

Let us introduce our model. Our model consists of two identical nanoclusters, each of which contains 236 "atoms" (Fig. 1). The clusters have facets due to the small number of "atoms". To construct one cluster, we first make the face-centered cubic crystal of $9 \times 9 \times 9$ layers of atoms. Next, we cut out a spherical cluster

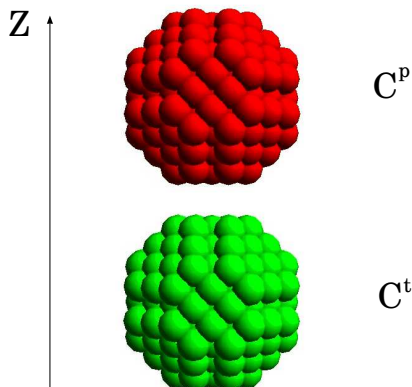


FIG. 1: (Color online) Snapshot of our model after equilibration to $T = 0.02\epsilon$. Each of them contains 236 "atoms" which are bound together by the modified Lennard-Jones potential.

from the cube. In Fig.1, we call the upper projectile and the lower target clusters C^p and C^t , respectively. All the atoms in one cluster are bound together by the modified

Lennard-Jones potential

$$U(r_{ij}) = 4\epsilon \left\{ \left(\frac{\sigma}{r_{ij}} \right)^{12} - c \left(\frac{\sigma}{r_{ij}} \right)^6 \right\}, \quad (1)$$

where r_{ij} is the distance between two arbitrary atoms i and j in this system, σ and ϵ are the core diameter and the scale of energy, respectively. Here, c is the cohesive parameter which changes the magnitude of cohesion between atoms. In our simulation, we adopt $c = 0.2$ between the atom i on the lower surface of C^p and the atom j on the upper surface of C^t while $c = 1$ between all the atoms in each cluster. Here the definition of the surface and the bulk atoms is as follows. Each cluster consists of 9 layers of atoms. We define the atoms outside the concentric inscribed sphere as the surface atoms while the other atoms as the bulk atoms. We assume that the surface atoms are different from the bulk atoms, which may cause the weak cohesive interaction between the clusters.[10, 22]

Let us introduce the volume fraction φ which is defined by

$$\varphi \equiv \frac{1}{6}\pi\rho\sigma^3, \quad (2)$$

where ρ is the number density. Figure 2 is the relation-

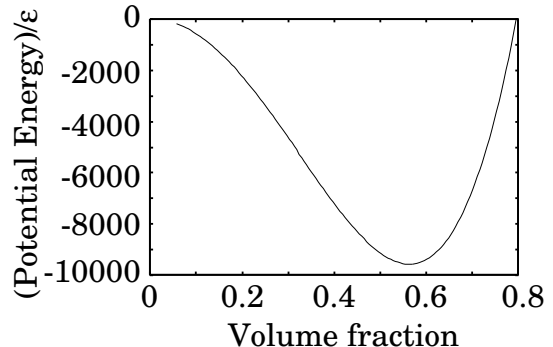


FIG. 2: Relationship between volume fraction of atoms and potential energy of one cluster.

ship between φ and the initial potential energy of one cluster. To construct a cluster, we adopt the value for φ as $\varphi = 0.56$ in which the potential energy is minimum, while we adopted $\varphi = 0.21$ in our previous work. [6]

The procedure of our simulation is as follows. As the initial condition of the simulation, the centers of mass of C^p and C^t are placed along the z -axis with the separation $4R$ between the centers of mass of C^p and C^t , where R is the radius of the cluster (Fig. 1). The two clusters are placed in mirror symmetric positions with respect to $z = 0$ so that a facet of one cluster is placed face-to-face with that of another cluster. We have checked that the relative rotational orientation of the clusters around z -axis little affect the relationship between the restitution coefficient and the colliding speed in our previous

work. [6] The initial velocities of the atoms in both C^p and C^t satisfies the Maxwell-Boltzmann distribution with the initial temperature T . The sample average is taken over different sets of initial velocities.

We numerically solve the equation of motion of each atom i described by

$$M \frac{d^2 \mathbf{x}_i}{dt^2} = \sum_{j \neq i} \mathbf{F}_{ij} + \sum_k \mathbf{F}_{ik}. \quad (3)$$

where M and \mathbf{x}_i are the mass of an atom and the position of the i -th atom, respectively. \mathbf{F}_{ij} is the modified Lennard-Jones force which is calculated from Eq. (1) as

$$\mathbf{F}_{ij} = -\frac{\partial U(r_{ij})}{\partial \mathbf{r}_{ij}}. \quad (4)$$

Numerical integration of the equation of motion for each atom is carried out by the second order symplectic integrator with the time step $dt = 1.0 \times 10^{-2} \sigma / \sqrt{\epsilon/M}$. To reduce computational costs, we introduce the cut-off length r_c of the Lennard-Jones interaction as $r_c = 2.5\sigma$. The rate of energy conservation, $|E(t) - E_0|/|E_0|$, is kept within 10^{-5} , where E_0 is the initial energy of the system and $E(t)$ is the energy at time t .

We equilibrate the clusters by using the velocity scaling method [30, 31] as the thermostat in the initial 2000 simulation steps. Here, we introduce the kinetic temperature,

$$T = \frac{2}{3N} \sum_i \frac{1}{2} M (\mathbf{v}_i - \mathbf{v}_c)^2, \quad (5)$$

where N and \mathbf{v}_c are the number of atom and the velocity of the center of mass of one cluster, respectively. It has been confirmed that the temperature of the system converges on a desired temperature during the equilibration.

After the equilibration we give the translational velocity to C^p and C^t to make them collide against each other without the thermostat. We give the translational speed with the acceleration $g = 0.02\epsilon/(\sigma M)$. The typical value of the relative impact speed in our simulation is $V = 0.1\sqrt{\epsilon/M}$, which is slightly less than the thermal velocity of the system defined by $V_{th} = \sqrt{T/M}$ when $T = 0.02\epsilon$.

III. SIMULATION RESULTS

A. Macroscopic Properties

Here we show the macroscopic properties of the colliding nanoclusters in our simulation. To characterize the rebound behavior of macroscopic inelastic collisions, we calculate the restitution coefficient e defined by

$$e = \frac{V_z(\bar{t}^*)}{V_z(0)}, \quad (6)$$

where $V_z(\bar{t}^*)$ is the z component of the relative translational speed of C^p to C^t , and \bar{t}^* is the scaled time of separation of the clusters, $\bar{t}^* \equiv t^*/(\sigma/\sqrt{\epsilon/M})$. We define the time of separation t^* by the time when the relative rebound speed becomes stable after the collision.

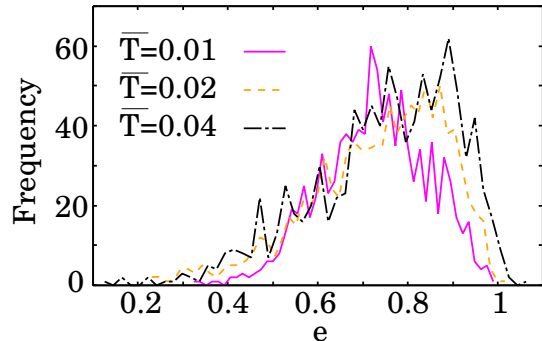


FIG. 3: (Color online) Histogram of e for several temperatures of clusters with $V_z = 0.2\sqrt{\epsilon/M}$.

Figure 3 shows the histograms of e for initial temperatures $T = 0.01\epsilon, 0.02\epsilon$, and 0.04ϵ , respectively. Each histogram is constructed from 1000 samples with the initial speed of $V_z = 0.2\sqrt{\epsilon/M}$. We find 12 samples of the super rebound at $T = 0.04\epsilon$ while all samples are the ordinary rebounds at $T = 0.01\epsilon$. At $T = 0.02\epsilon$ we found that only 1 sample is the super rebound. On the other hand, if we adopt $V_z = 0.3\sqrt{\epsilon/M}$, most of the rebounds are ordinary. We can find only two samples of super rebounds even at $T = 0.04\epsilon$. Thus, the super rebounds can be observed only if the colliding speed is lower or almost equal to the thermal speed.

B. Thermodynamic Properties

Here we show the time evolution of kinetic temperature defined by Eq.(5). Figure 4 shows typical examples of the changes in temperature in an ordinary rebound and a super rebound. \bar{t} is the scaled time, $\bar{t} \equiv t/(\sigma/\sqrt{\epsilon/M})$. A slight discrepancy in temperature between C^p and C^t is observed after the equilibration in Fig. 4 (a). The temperature increases after the collision around $\bar{t} = 9$ for an ordinary rebound (see Fig. 4(a)), where a part of the translational energy is converted to the internal energy. On the other hand, the temperature decreases in C^t while the temperature of C^p increases after the collision for a super rebound (Fig. 4(b)).

Next let us investigate the entropy change ΔS defined by Eq. (A9) in Appendix A. Figure 5(a) plots the time evolution of ΔS for C^p and C^t in a super rebound, which shows that the entropy increases in C^t while it decreases in C^p during collision for $\bar{t} < 15.8$. On the other hand, Figure 5(b) shows that the discrepancy of entropy change remains finite after the collision for $\bar{t} > 15.8$. In addition,

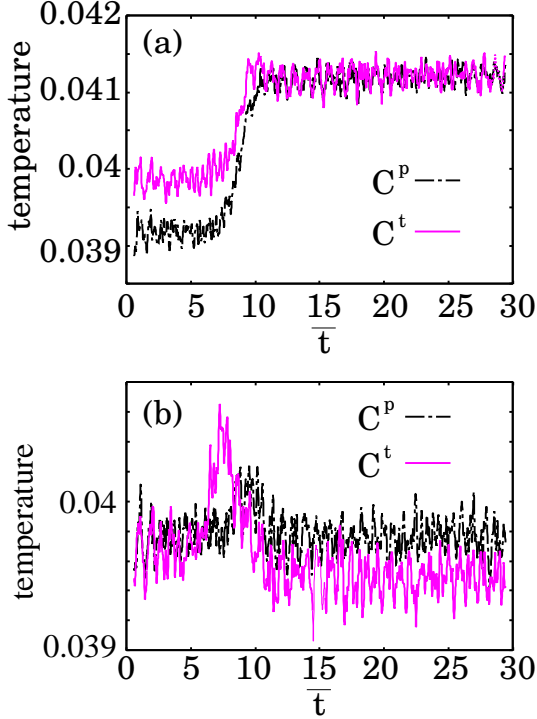


FIG. 4: (Color online) Time evolution of temperature for (a) an ordinary rebound and (b) a super rebound.

it is remarkable that the entropy of C^t decreases corresponding to the decrease of temperature.

So far, we have reported the results of our simulation on thermodynamic quantities. What we confirm is that the behavior of such quantities in super rebounds is seemingly in contrast to what is expected from the second law of thermodynamics. However, we should note that the second law is only strictly valid after ensemble average is taken over. In this sense, our result does not violate the second law of thermodynamics.

C. Structural Change during Collision

Let us investigate the structural change of the clusters induced by collisions. To characterize the structural change, we first introduce a local bond order parameter known as time-averaged Steinhart's bond order parameter Q_i (see Eq.(B3) for its explicit definition). [29, 32, 33] We note that Steinhart's bond order parameters are used to characterize the structural change in nanoclusters associated with collisions[34] and melting[35, 36] as well as equilibrium structures of crystalline solids. According to the definition of the bond order parameter summarized in Appendix B, we calculate $Q_4(i)$ and $Q_6(i)$ of each atom i before and after collisions, respectively. For the time average in calculation of $Q_4(i)$ and $Q_6(i)$, we use $t_b = 5.5\sigma/\sqrt{\epsilon/M}$ and $t_a = 20\sigma/\sqrt{\epsilon/M}$ for before

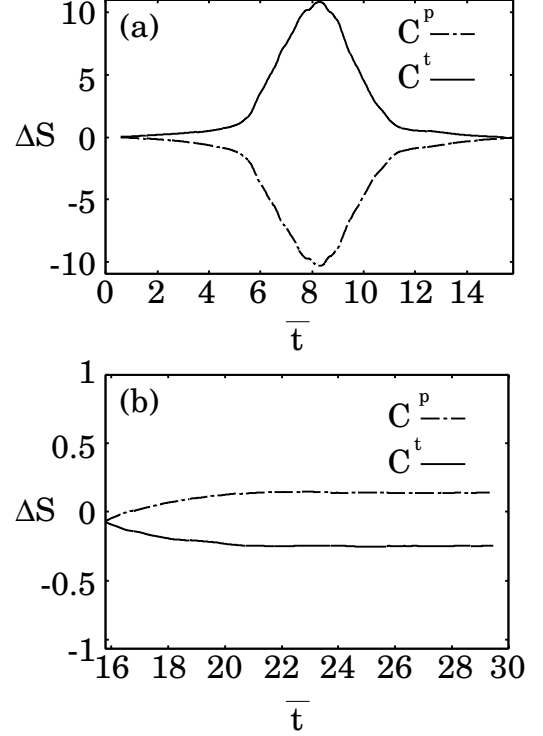


FIG. 5: Time evolution of ΔS of a super rebound in (a) $\bar{t} \leq 15.8$ and (b) $\bar{t} \geq 15.8$. Chain and solid lines show ΔS in C^p and C^t , respectively. At $\bar{t} = 30$, ΔS of C^t becomes -0.243 .

TABLE I: Numbers of FCC “atoms” for ordinary rebound.

	numbers of FCC “atoms”	Q_4	Q_6
before collision	649	0.19105	0.56897
after collision	574	0.1908	0.5689

and after collisions, respectively, with the time interval $\tau_\alpha = 1.5\sigma/\sqrt{\epsilon/M}$, where t_a and t_b respectively correspond to t_0 in Eq. (B3).

On Q_4 - Q_6 plane, the highest peak can be found around $(Q_4, Q_6) = (0.190, 0.574)$ which is characteristic for FCC crystal structure. We cannot find visible shift of the peak position on Q_4 - Q_6 plane during the collision in both super and ordinary rebounds. However, we find that the number of “atoms” at the highest peak decreases after the collision for ordinary rebounds, which means that the number of “atoms” in FCC bond order decreases after the collision (see Table I). On the contrary, for super rebounds, the number of “atoms” at the highest peak increases after the collision, which means that the FCC bond order becomes intensive after the collision. Thus, the super rebounds are characterized by the increase of the number of “atoms” with FCC bond order during collisions.

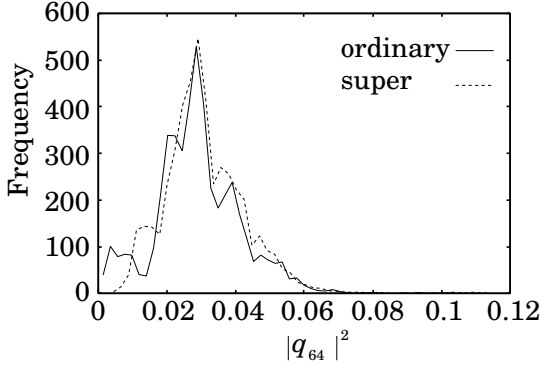
To investigate the details of the structural change, we

TABLE II: Numbers of FCC “atoms” for super rebound.

	numbers of FCC “atoms”	Q_4	Q_6
before collision	690	0.1890	0.5735
after collision	718	0.1911	0.5692

also calculate the distribution of $|q_{6m}(i)|^2$ defined by Eq. (B1). To construct these distributions, we use the particle data at the final instant of the initial thermalization by the velocity scaling method. Because q_{lm} is equal to $(-1)^m q_{lm}^*$, we only investigate the case of $m \geq 0$.

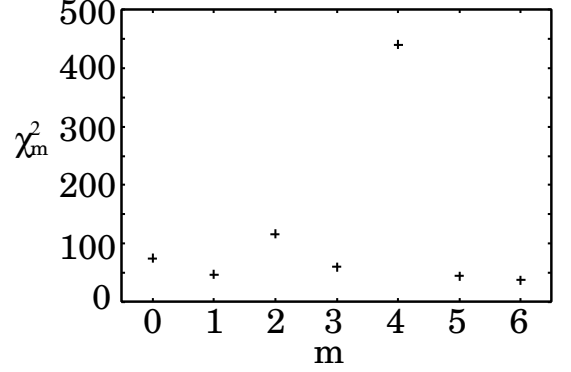
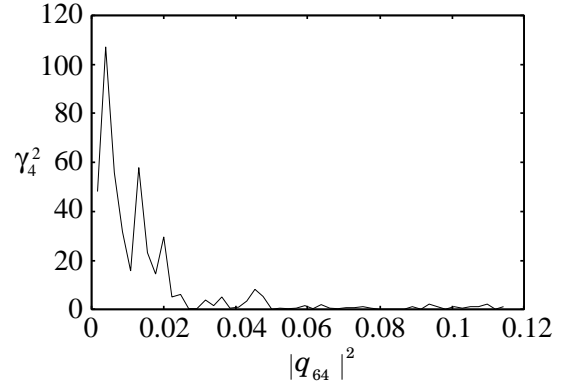
We present the histogram of $|q_{64}(i)|^2$ in Fig. 6. The solid curve represents the frequency distribution for ordinary rebounds while the broken curve is that for super rebounds. One can find the slight discrepancy between those two distributions. We should mention that the discrepancy is invisible for the other m , though we do not present the corresponding figures.

FIG. 6: Histogram of $|q_{64}|^2$.

To quantify the discrepancy between those two distributions, we introduce χ_m^2 defined by

$$\chi_m^2 = \sum_j \frac{(O_m(j) - S_m(j))^2}{O_m(j) + S_m(j)} \equiv \sum_j \gamma_m^2(j), \quad (7)$$

where $O_m(j)$ and $S_m(j)$ are the frequencies of $|q_{6m}(i)|^2$ in the j -th bin for ordinary and super rebounds, respectively. We calculate χ_m^2 for each value of m to investigate the relationship between m and χ_m^2 . Figure 7 shows the relationship between m and χ_m^2 , which characterizes the difference between super rebounds and ordinary rebounds. This figure shows that the discrepancy between the distributions of $|q_{64}(i)|^2$ is remarkably large compared to other values of m . In addition, we show the relationship between $\gamma_4^2(j)$ introduced in Eq.(7) and $|q_{64}(i)|^2$ in Fig. 8, where a remarkable difference can be found in the range of $|q_{64}(i)|^2 \leq 0.02$.

FIG. 7: Relationship between m and χ_m^2 which is defined by Eq. (7).FIG. 8: γ_4^2 as function of $|q_{64}(i)|^2$.

IV. DISCUSSION

Let us discuss our results. In the previous section, we have demonstrated that the structural difference of clusters can be found between the super and the ordinary rebounds. Here we investigate the potential energy of the characteristic local structures included in the clusters which induce the super rebounds.

Focusing on the noticeable peaks in Fig. 8, we select the “atoms” with the order in the range, $1.1643 \times 10^{-2} \leq |q_{64}(i)|^2 \leq 1.7425 \times 10^{-2}$, from 20 clusters which induce the super rebounds. The reason why we choose the range of $|q_{64}(i)|^2$ is as follows. The characteristic peaks in Fig. 8 are characterized by $|q_{64}(i)|^2 = (1.4534 \pm 0.2891) \times 10^{-2}$, so that we pick up “atoms” in the above range. For each of the selected “atoms”, we define the neighboring “atoms” which are located within the distance of 1.6σ . We define a local structure by the collection of the selected atom and its neighboring “atoms”. Figure 9 is a snapshot of a cluster including two local structures, each of which is centered by the atom which has the order (red or medium grey). This figure shows that the local structures are located on the surface of the cluster. Moreover,

the local structures seem to be unstable due to the less-ordered orientation of “atoms”, which may lead to the high potential energy.

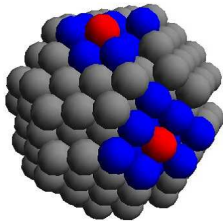


FIG. 9: (Color online) Cluster which induces super rebounds. Red (medium grey) particles show the “atoms” with the order $1.1643 \times 10^{-2} \leq |q_{64}(i)|^2 \leq 1.7425 \times 10^{-2}$ while blue (dark grey) particles are neighboring “atoms”.

Next, we calculate the averaged potential energy of those local structures. For the purpose, we calculate the potential energy of each atom in the cluster with the cutoff 3.5σ and sum up the potential energy over all the “atoms” in a local structure to obtain its potential energy. Among 20 clusters which induce super rebounds, we find 372 “atoms” to satisfy $1.1643 \times 10^{-2} \leq |q_{64}|^2 \leq 1.7425 \times 10^{-2}$, by which we calculate the averaged potential energy of one local structure. From our calculation, the averaged potential energy per one local structure becomes -97.827ϵ .

For comparison, we focus on the potential energy of the local structure which belongs to the highest peak in Fig. 6 because we find same number of the local structures both in super rebounds and in ordinary rebounds. The local structure in this case is defined by the collection of the “atoms” with the order around the peak, $2.8 \times 10^{-2} \leq |q_{64}|^2 \leq 3.0 \times 10^{-2}$, and its neighboring “atoms” in the clusters which induce the super and the ordinary rebounds. From the calculation with 482 local structures in the clusters which induces super rebounds, we obtain the averaged potential energy per one local structure as -104.814ϵ . In the case of the clusters which induce ordinary rebounds, the averaged potential energy becomes -104.202ϵ from the calculation of 512 local structures.

From these results, the clusters for the super rebound has more metastable local structures with high potential energy rather than the clusters for the ordinary rebound. Thus, we conjecture that a part of the high potential energy is transferred to the macroscopic degrees of freedom during the super-rebound collision. Moreover, we can also conjecture that the decreases of temperature and entropy after collision are connected with the decrease of the potential energy. In this paper, we focus on the relationship between the local structure and the super rebound. It is also important to understand the role of macroscopic structural change. The macroscopic deformation of nanoclusters after the collision will be reported elsewhere.[37]

V. CONCLUSION

In this paper, we have performed the molecular dynamics simulation of colliding nanoclusters to study the origin of super rebounds. Through the investigation of the thermodynamic properties, we have found that the decreases of the temperature and the entropy are observed in one of the binary clusters when the super rebound is observed. This may be attributed to the biased distribution of the local bond order parameters after the collision which is caused by the initial metastable configuration of “atoms”.

Through the investigation of the local bond order parameters, we have found the discrepancy of the distributions of the order $|q_{64}(i)|^2$ between the super and the ordinary rebounds. The averaged potential energy of the local structure which belongs to the characteristic peak in the $|q_{64}(i)|^2$ distribution is larger than the typical local structures which are abundant in our cluster. Thus, the energy transfer from the local structure to the macroscopic degree of freedom accompanied by the structural change during collision play an important role in super rebounds. Moreover, the change of entropy associated with the change in the internal state of order after the collision is the key point for understanding the emergence of the super rebounds. Further investigation of the relationship between the local structural change and the entropy decrease will be one of our future tasks.

Acknowledgments

We would like to thank N. V. Brilliantov, T. Kawasaki, S. Takesue, R. Murakami, and K. Saitoh for their valuable comments. Also, HK would like to thank Y. Wang and W. Lechner who gave him many advises for calculation of order parameters and how to use their calculation codes. Parts of numerical computation in this work were carried out at Yukawa Institute Computer Facility. This work was supported by the Grant-in-Aid for the Global COE Program “The Next Generation of Physics, Spun from Universality and Emergence” from the Ministry of Education, Culture, Sports, Science and Technology (MEXT) of Japan.

Appendix A: Calculation of entropy

In this appendix, we explain the method to calculate the entropy in our system. Let us assume that the collision of C^p onto C^t does the work δW and changes the internal energy of C^t . Because each cluster is an isolated system, we assume that the change in heat δQ of C^t is determined by the first law of thermodynamics,

$$\delta Q = dE + \delta W, \quad (A1)$$

where dE is the change in the internal energy.

The internal energy E is calculated as

$$E = \sum_i \frac{\mathbf{p}_i^2}{2m} + \frac{1}{2} \sum_i \sum_{j \neq i} U(r_{ij}), \quad (\text{A2})$$

where \mathbf{p}_i , m are the relative momentum of an atom in C^t against the center of mass and the mass of an atom, respectively. $U(r_{ij})$ is the potential energy between the “atoms” i and j in C^t .

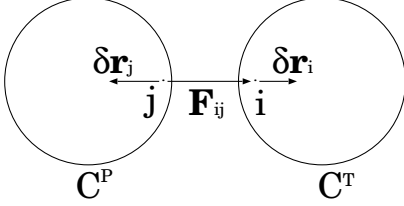


FIG. 10: Interaction between an atom in C^t and an atom in C^p .

The amount of work $\delta W(t)$ acting on C^t is defined as follows. Let us define the work done by the atom j of C^p to the atom i of C^t (Fig. 10). Assuming that the displacements of the “atoms” are caused by the interactive force \mathbf{F}_{ij} , the amount of work $\delta W_{ij}(t)$ done by the atom j to the atom i during an interval dt may be written as

$$\delta W_{ij}(t) = \mathbf{F}_{ij} \cdot [\mathbf{r}_{ij}(t+dt) - \mathbf{r}_{ij}(t)], \quad (\text{A3})$$

where $\mathbf{r}_{ij}(t) = \mathbf{r}_i(t) - \mathbf{r}_j(t)$. Thus, the work $\delta W(t)$ done by C^p to C^t may be expressed as

$$\delta W(t) = \frac{1}{2} \sum_i \sum_j \delta W_{ij}(t). \quad (\text{A4})$$

Using these quantities, we define the entropy difference $\Delta S(t) = S(t) - S(0)$ as

$$\Delta S(t) = \int_0^t \frac{\delta Q(t')}{T(t')} dt'. \quad (\text{A5})$$

Here we use the kinetic temperature Eq.(5) as T . To calculate $\Delta S(t)$ by Eq.(A5), we first smooth the temperature and the heat as

$$\tilde{T}(t) = \int_{t-\Delta t}^{t+\Delta t} T(t') dt' \quad (\text{A6})$$

$$\delta \tilde{Q}(t) = \int_{t-\Delta t}^{t+\Delta t} \delta Q(t') dt' \quad (\text{A7})$$

$$(\text{A8})$$

with $\Delta t = 0.565\sigma/\sqrt{\epsilon/m}$ because those data change rapidly against time. By using those smoothed parameters, the entropy change of C^t may be rewritten as

$$\Delta S(t) = \int_0^t \frac{\delta \tilde{Q}(t')}{\tilde{T}(t')} dt', \quad (\text{A9})$$

where we adopt the simple trapezoidal rule for the evaluation of the integral.

TABLE III: Bond orientational order parameters for fcc, bcc, and hcp crystals[32].

	q_4	q_6
fcc	0.191	0.575
bcc	0.036	0.511
hcp	0.097	0.485

Appendix B: Calculation of order parameter

In this appendix, we introduce Steinhardt’s order parameter to characterize the structure of our model [29, 32, 33]. Let us assume that an atom i in a crystalline structure is surrounded by $N_b(i)$ “atoms” within the cutoff length r_c . That is, the distance r_{ij} between the i -th atom and one of the neighboring “atoms” j is less than the cutoff length r_c . In our analysis, we adopt $r_c = 1.6\sigma$.

First, for each atom, we calculate the average of spherical harmonics which depends on r_{ij} as follows:

$$q_{lm}(i) = \frac{1}{N_b(i)} \sum_{j=1}^{N_b(i)} Y_{lm}(r_{ij}). \quad (\text{B1})$$

Next, we introduce $q_l(i)$ according to the following definition:

$$q_l(i) = \sqrt{\frac{4\pi}{2l+1} \sum_{m=-l}^l |q_{lm}(i)|^2}. \quad (\text{B2})$$

Instead of $q_l(i)$, we use the time-averaged value defined by

$$Q_l(i) = \frac{1}{\tau_\alpha} \int_{t_0}^{t_0+\tau_\alpha} q_l(i) dt \quad (\text{B3})$$

with the time interval τ_α .

Each crystalline structure, such as a body-centered cubic (bcc) and a face-centered cubic (fcc), has a characteristic distributions of those parameters. For example, the distributions of q_4 and q_6 in a fcc structure shows two peaks while the distributions in other structure has a single peak in a Lennard-Jones system.[33] The mean values of those distributions are summarized in Table III.[32]

-
- [1] T. L. Hill, *Thermodynamics of Small Systems*, Part I and II (Benjamin, Amsterdam, 1964).
- [2] F. Baletto and R. Ferrando, *Rev. Mod. Phys.* **77**, 371 (2005).
- [3] A. I. Ayesh, S. A. Brown, A. Awasthi, S. C. Hendy, P. Y. Convers, and K. Nichol, *Phys. Rev. B* **81**, 195422 (2010).
- [4] A. Awasthi, S. C. Hendy, and S. A. Brown, *Math. Mech. Sol.* **15**, 771 (2010).
- [5] L. B. Han, Q. An, S. N. Luo, and W. A. Goddard III, *Material Lett.* **64**, 2230 (2010).
- [6] H. Kuninaka and H. Hayakawa, *Phys. Rev. E* **79**, 031309 (2009).
- [7] K. Saitoh and H. Hayakawa, *Prog. Theor. Phys.*, **122**, 1081 (Kyoto Univ. 2009), and references therein.
- [8] M. Suri and T. Dumitrică, *Phys. Rev. B* **78**, 081405R (2008).
- [9] S. J. Antony, R. Moreno-Atanasio, J. Musadaidzwa, and R. A. Williams, *J. Nanomaterials.*, no. 125386, 1 (2008).
- [10] A. Awasthi, S. C. Hendy, P. Zoontjens, S. A. Brown, and F. Natali, *Phys. Rev. B*, **76**, 115437 (2007).
- [11] M. Kalweit and D. Drikakis, *Phys. Rev. B*, **74**, 235415 (2006) and references therein.
- [12] M. Kalweit and D. Drikakis, *J. Compt. Theor. Nanoscience* **1**, 367 (2004).
- [13] A. Tomsic, H. Schröder, K. L. Kompa K. L., and C. R. Gebhardt, *J. Chem. Phys.* **119**, 6314 (2003).
- [14] Y. Yamaguchi and J. Gspann, *Phys. Rev. B*, **66**, 155408 (2002).
- [15] W. Harbich, *Metal Clusters at Surfaces*, ed. by Karl-Heintz, Meiwes-Broer, p.p.107 (Springer, Berlin, 2000).
- [16] P. Valentini and T. Dumitrică, *Phys. Rev. B*, **75**, 224106 (2007).
- [17] O. Knospe and R. Schmidt, *Theory of atomic and molecular clusters*, ed. by J. Jellinek, 111 (Springer, Berlin, 1999).
- [18] L. Ming, N. Markovic, M. Svanberg, and J. B. C. Pettersson: *J. Phys. Chem. A* **101**, 4011 (1997).
- [19] N. V. Brilliantov, N. Albers, F. Spahn, and T. Pöschel, *Phys. Rev. E* **76**, 051302 (2007).
- [20] S. Kim, *Phys. Rev. E* **83**, 041302 (2011).
- [21] P. Kosinski and A. C. Hoffmann, *Phys. Rev. E* **84**, 031303 (2011).
- [22] Y. Sakiyama, S. Takagi, and Y. Matsumoto, *Phys. Fluids*, **16**, 1620 (2004).
- [23] T. Hawa and M. R. Zachariah, *Phys. Rev. B* **71**, 165434 (2005).
- [24] K. Saitoh, A. Bodrova, H. Hayakawa and N. V. Brilliantov, *Phys. Rev. Lett.* **105**, 238001 (2010).
- [25] K. Saitoh and Y. Yonekawa, *J. Adv. Mech. Des. Sys. Man.*, **4**, 405 (2010).
- [26] M. Y. Louge and M. E. Adams, *Phys. Rev. E* **65**, 021303 (2002).
- [27] H. Kuninaka and H. Hayakawa, *Phys. Rev. Lett.* **93**, 154301 (2004).
- [28] C. Shen et al., *Nature Physics* advance online publication, 7 OCTOBER 2012 (DOI: 10.1038/NPHYS2440).
- [29] P. J. Steinhardt, D. R. Nelson, and M. Ronchetti, *Phys. Rev. B* **28**, 784 (1983).
- [30] L. V. Woodcock, *Chem. Phys. Lett.* **10**, 257 (1971).
- [31] S. Nosé, *Prog. Theor. Phys. Suppl.* **103**, 1 (1991).
- [32] J. S. van Duijneveldt and D. Frenkel: *J. Chem. Phys.* **96**, 4655 (1992).
- [33] W. Lechner and C. Dellago, *J. Chem. Phys.* **129**, 114707 (2008).
- [34] S. -C. Jung, D. Suh, and W. -S. Yoon, *J. Aero. Sci.* **41**, 745 (2010).
- [35] S. K. R. S. Sankaranarayanan, V. R. Bhethanabotla, and B. Joseph, *Phys. Rev. B* **71**, 195415 (2005).
- [36] Y. Wang, S. Teitel, and C. Dellago, *J. Chem. Phys.* **122**, 214722 (2005).
- [37] R. Murakami and H. Hayakawa, to be published.